New layer method for the investigation of the electronic properties of two-dimensional periodic spatial structures: First applications to copper and aluminum

G. Wachutka
Sektion Physik der Universität München, D-8000 Munich 2, Federal Republic of Germany
(Received 31 March 1986)

A new formalism, the "assembly of boundary-controlled monolayers" (ABCM) method, has been developed for the calculation of the electronic structure of general three-dimensional physical systems exhibiting two-dimensional translational symmetry. By outlining the underlying basic concepts, it is shown that there is indeed no physically relevant restriction with regard to the form of the electronic potential nor to the number of layers of which the structure is composed. It is characteristic of the method that, in a first step, the properties of each monolayer of the structure considered are represented by a Green's operator; then, by application of the "layer composition process" to these operators, the entire structure is synthesized. Special interest is paid to the case of a crystal surface; it is shown that the ABCM method provides direct access to the complex band structure, and enables a natural classification of the electronic states of a half-crystal. A first numerical realization of the method was used to demonstrate its reliability in practical applications: Thusly have comprehensive investigations of the complex band structure and of the surface states and resonances of the Al(100), Al(110), and Cu(100) surfaces been performed. These calculations are not only high-accuracy refinements of previous work, but they also provide the missing continuation in regions of $(\mathbf{k},E)$ space where no theoretical results have been obtained up to now, hereby yielding confirmation of some speculative interpretations of the experimental data.

I. INTRODUCTION

For the calculation of the electronic structure of physical systems exhibiting two-dimensional (2D) translational symmetry [such as, e.g., multilayers, thin films, or a semi-infinite crystal with a (possibly) reconstructed and relaxed surface], various computational methods have been proposed, which may be classified as follows: First, there is the group of those methods which had originally been developed for the calculation of the electronic properties of the three-dimensional infinite crystal (linear combination of atomic orbitals, linear combination of Gaussian orbitals, linear combination of muffin-tin orbitals, and linearized augmented plane waves);[1-9] they were made applicable to systems with only two-dimensional translational symmetry by a proper modification of the trial functions, taking into account the asymptotic behavior of the wave function outside the crystal layers. It is an intrinsic feature of all of those methods that the number of trial functions which must be included in the calculation is proportional to the number of layers considered. Therefore, only a relatively small sequence of layers (10—20) can be handled, even if a modern computer with large storage is available.

This crucial restriction to only thin multilayers can be avoided by using a so-called monolayer method. Here, the given layered structure is subdivided into monolayers $z_L^{(i)} \le z \le z_R^{(i)}$ ($i=1,2,3,\ldots$; z denotes the coordinate perpendicular to the planes of 2D-translational symmetry), and Schrödinger's equation—subject to certain boundary conditions at $z=z_R^{(i)}$ and/or $z=z_L^{(i)}$—is solved within any single layer. Then, in a second step, the wave function ψ for the whole structure is determined by matching the boundary values of ψ at $z=z_R^{(i)}$ and/or $z=z_L^{(i)}$. The propagation-matrix method[10-12] and the transfer-matrix method[13,11,14] are based on a one-sided boundary condition for ψ and its z derivative $\partial_z\psi$ at $z=z_L^{(i)}$; this ensures, indeed, a quite simple formulation of the matching condition at the cross sections $z=z_L^{(i)}$, but unfortunately corresponds to an improperly posed problem in the mathematical sense.[15,16] Hence, even though the successful application to simple metals and high-symmetric surfaces[17,18] seemed to prove the reliability of these methods, it is not very surprising that numerical instabilities and lack of convergence were observed when the calculations were extended to more complex elements and to surfaces of less symmetry.[19,20]

A way to overcome these difficulties is to pose a two-sided boundary condition to a linear combination of ψ and $\partial_z\psi$ at both the "left" and the "right" cross sections of the monolayer; more precisely,

$$\Lambda\psi(\mathbf{r}_{||},z_X)+\partial_n\psi(\mathbf{r}_{||},z_X)=b_X(\mathbf{r}_{||}) \quad \text{for } X=R,L \ . \tag{1}$$

Here, b_R and b_L are prescribed boundary data at $z=z_R$ and $z=z_L$, respectively, which are determined in the further course of the calculation by matching them to the corresponding boundary values from the neighboring monolayers; Λ denotes a positive linear operator acting on $\mathbf{r}_{||}$, the coordinates perpendicular to z, and $\partial_n=(\mathbf{n}\cdot\mathbf{e}_z)\partial_z$ denotes the outward normal derivative. As was shown by the author,[15] boundary conditions of type (1) imply a properly posed mathematical problem such that instabilities and divergencies are to be excluded. The well-established layer-KKR (Korringa-Kohn-Rostoker) method,[21] which proved to be a solid basis for low-energy

electron diffraction (LEED) calculations,[22,23] and related Green's-function methods underlying angle-resolved photoemission calculations[24,25] make use of boundary conditions of this form.[26] However, the electronic potential has to be supposed to exhibit only a simple z dependence outside and a mere muffin-tin form inside the layered structure. As a matter of fact, the formulation of the layer-KKR method crucially depends on the latter assumption, and non-muffin-tin corrections to the potential may be included at most by perturbation theory.[27]

In order to eliminate all of the restrictions described above, the ABCM method (assembly of boundary controlled monolayers[15]) has been developed as a new scheme. Since it is a layer method using the boundary condition (1), it could be based on rigorous mathematical foundations securing convergence and stability. It may be applied to any square-integrable potential; thus, it is designed especially to enable real self-consistent calculations without any physically relevant confinement to a special class of potentials. So, for instance, it is flexible enough to allow for the relaxation of the electronic structure near the crystal surface. Nevertheless, restricting the general form of the potential yields a considerable reduction of computational work. The numerical realization of the ABCM method presented in this paper was primarily intended to put the abstract formalism to the test on physical structures and, therefore, it should provide the possibility of immediately comparing the results with those of previous calculations obtained by other methods (based on muffin-tin potentials). Hence, as a first step, a computer program was designed and implemented which is applicable to potentials of so-called warped muffin-tin form. In the following sections numerical results for Al and Cu are given, after some basic concepts have been introduced which are necessary for the understanding of the formalism.

II. BASIC CONCEPTS

Since the functional-analytical framework of the method will be published in another paper, the underlying concepts are introduced without going into mathematical details. Let Z denote a two-dimensional unit cell in a plane of 2D-translational symmetry; then, a monolayer is represented by an elementary region $\Omega = Z \times (z_L, z_R)$ together with an electronic potential $w(\mathbf{r}_{||}, z)$ defined on Ω. The monolayer problem consists of finding the general solution to the single-particle Schrödinger equation in Ω subject to a planar Bloch condition characterized by a two-dimensional propagation vector $\mathbf{k}_{||}$. In order to achieve this aim, an additional boundary condition of type (1) is posed, with Λ being set proportional to the square root of the planar kinetic energy operator: $\Lambda = \alpha(-\partial_x^2 - \partial_y^2 + E_0)^{1/2}$. Provided α and E_0 are (arbitrarily chosen) positive numbers, it can be shown that for any given energy E,[28] propagation vector $\mathbf{k}_{||}$, and boundary function $b = (b_R, b_L)$ a unique solution to Schrödinger's equation exists and depends continuously on the data $(E, \mathbf{k}_{||}, b)$, i.e., the monolayer problem is properly posed. The mapping $b \mapsto \psi_b$ is described by a linear operator

$$\psi_b = G_{E,\mathbf{k}_{||}} b \ , \tag{2}$$

which is called the monolayer Green's operator. By varying b (in an appropriately chosen function space), any special solution for the given values of E and $\mathbf{k}_{||}$ may be obtained. Hence, the monolayer Green's operator $G_{E,\mathbf{k}_{||}}$ has to be regarded as a mathematical object which characterizes the totality of (single-particle) electronic phenomena within one monolayer.

It can especially be used to describe the transmission and reflection properties in the following way: Given boundary data (b_R, b_L), the Green's operator $G_{E,\mathbf{k}_{||}}$ yields the boundary values of the wave function $\psi_R(r_{||}) := \psi(r_{||}, z_R)$ and $\psi_L(r_{||}) := \psi(r_{||}, z_L)$; instead of ψ_R and ψ_L, it is more convenient to consider

$$c_R := \Lambda\psi_R - \partial_n\psi_R, \quad c_L := \Lambda\psi_L - \partial_n\psi_L \ . \tag{3}$$

The boundary values $c = (c_R, c_L)$ depend linearly on b (via $G_{E,\mathbf{k}_{||}}$):

$$\begin{bmatrix} c_R \\ c_L \end{bmatrix} = S_{E,\mathbf{k}_{||}} \begin{bmatrix} b_R \\ b_L \end{bmatrix} = \begin{bmatrix} \mathscr{R}_R - 1 & \mathscr{T}_{RL} \\ \mathscr{T}_{LR} & \mathscr{R}_L - 1 \end{bmatrix} \begin{bmatrix} b_R \\ b_L \end{bmatrix} . \tag{4}$$

$S_{E,\mathbf{k}_{||}}$ is called the monolayer scattering matrix (not to be confused with the layer-KKR scattering matrix!); its coefficients are linear operators and may be computed from $G_{E,\mathbf{k}_{||}}$ in an obvious way. It is worth pointing out that in (4) the application of $S_{E,\mathbf{k}_{||}}$ to (b_R, b_L) yields functions (c_R, c_L) which belong to the same class of functions as b_R and b_L. Therefore, if b_R and b_L are well-behaved functions, so are c_R and c_L, in contrast to the propagation-matrix method mentioned above, where by each application of the propagation matrix, the quality of the resulting functions degenerates.[15]

Having calculated the S matrices for each monolayer of the structure considered, any two neighboring layers, A and B, can be combined to the composite layer AB by means of the "layer composition equations" which may be represented most appropriately in the form of the diagram shown in Fig. 1. Given $S^{(A)}$ and $S^{(B)}$, this set of equations yields the coefficients $\mathscr{R}$ and $\mathscr{T}$ of the layer scattering matrix $S^{(AB)}$. Although it involves nonlinear operations (e.g., the inversion of linear operators), it is a well-conditioned system of equations such that no numerical problems arise. By repeated application of this layer composition process, the entire structure can be synthesized.

In what follows, let us restrict ourselves to the special case of a half-crystal. Here, only in a confined region $z_V \le z \le z_B$ near the surface may neighboring monolayers

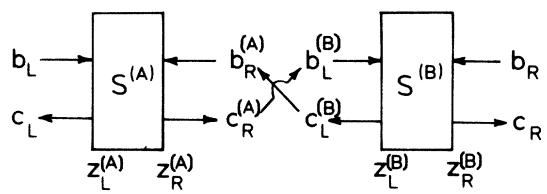

FIG. 1. Graphical illustration of the layer composition process.

be different, whereas in the bulk $z_B \le z$, all layers are identical. Therefore, it is advantageous to make use of the "layer-doubling method" analogous to that in LEED theory,[29,30] in order to construct the bulk scattering matrix; thus, starting from a single bulk layer, it takes only n reduplications to generate a bulk region of 2^n layers. It was shown by the author[15] that the rate of convergence crucially depends on E and $\mathbf{k}_{||}$, and that it may be expressed in terms of the "complex band structure" as will be discussed below.

Suppose the matrix $S^c_{E,\mathbf{k}_{||}}$ of the composite structure $z_V \le z \le z_B + 2^n d$ (d = width of a bulk monolayer) has been calculated; then, the general solution to Schrödinger's equation matching the asymptotic behavior of the wave function in the column $Z \times (-\infty, +\infty)$ can be determined in the following way: In the bulk, the wave function is represented as an infinite linear combination of so-called generalized Bloch waves $\psi^{(\mu)}_{E,\mathbf{k}_{||}}$ ($\mu = 1,2,3,\ldots$) which include both "propagating waves" with real (three-dimensional) propagation vector $\mathbf{k} = \mathbf{k}_{||} + k^{(\mu)}_{\perp}\mathbf{e}_z$ ($k^{(\mu)}_{\perp} \in R$) and "evanescent waves" with complex z component $k^{(\mu)}_{\perp} \in C$.[31] Within the framework of the ABCM formalism the generalized Bloch waves are to be calculated by solving the general linear eigenvalue problem

$$\begin{bmatrix} \mathscr{R}_R - 1 & \mathscr{T}_{RL} \\ 1 & 0 \end{bmatrix} \begin{bmatrix} b_R \\ b_L \end{bmatrix} = tT \oplus T \begin{bmatrix} 0 & 1 \\ \mathscr{T}_{LR} & \mathscr{R}_L - 1 \end{bmatrix} \begin{bmatrix} b_R \\ b_L \end{bmatrix} . \tag{5}$$

Here, the coefficients $\mathscr{R}$ and $\mathscr{T}$ are to be taken from the bulk monolayer scattering matrix according to (4); T denotes the operator of translation by the parallel component $\mathbf{a}_{3||} = (1 - \mathbf{e}_z \otimes \mathbf{e}_z)\mathbf{a}_3$ of a three-dimensional primitive lattice vector $\mathbf{a}_3$, such that $Z + (0,1)\mathbf{a}_3$ is a primitive unit cell of the bulk crystal, and the complex eigenvalue t is related to the (generally complex) propagation vector $\mathbf{k}$ by $t = \exp(i\mathbf{k}\cdot\mathbf{a}_3)$. If desired, the generalized Bloch waves $\psi^{(\mu)}_{E,\mathbf{k}_{||}}$ may be explicitly obtained by applying the Green's operator $G_{E,\mathbf{k}_{||}}$ to the eigenvectors $(b^{(\mu)}_R, b^{(\mu)}_L)$. Eigenvalues $t^{(\mu)}$ with $|t^{(\mu)}| = 1$ correspond to the bulk band structure (propagating waves), whereas $|t^{(\mu)}| \neq 1$ represents a point $(E,\mathbf{k})$ located at one of the "real lines" of the complex band structure (evanescent waves).[32] As can be concluded from the law of conservation of probability current,[33,15] the (finite) number $\sigma(E,\mathbf{k}_{||})$ of waves propagating into the half-crystal equals that of those being radiated; hence, by increasing the number of bulk layers, the wave function $\psi^{(B)}$ deep inside the bulk region ($z \ge z_B + 2^n d$) will resemble a finite linear combination of $2\sigma(E,\mathbf{k}_{||})$ propagating waves

$$\psi^{(B)} = \sum_{\mu=1}^{2\sigma} \alpha_\mu(E,\mathbf{k}_{||})\psi^{(\mu)}_{E,k_{||}} , \tag{6}$$

since all evanescent waves are to be neglected there.

In the vacuum region $z \le z_V$ outside the half-crystal the electronic potential may be assumed to depend only on the z coordinate. Therefore, the wave function is appropriately represented in the form of a planar Fourier expansion[34] with z-dependent Fourier coefficients

$$\psi^{(V)}(\mathbf{r}) = \sum_{\mathbf{g} \in G^*_2} u(\eta_\mathbf{g}, z)\exp[i(\mathbf{k}_{||} + \mathbf{g})\cdot\mathbf{r}_{||}] \tag{7}$$

(G^*_2 is the two-dimensional reciprocal lattice; $-\eta_\mathbf{g} = E - |\mathbf{k}_{||} + \mathbf{g}|^2 =$ energy in the z direction per $\mathbf{g}$ vector), which are to be calculated either analytically or numerically by solving a one-dimensional Schrödinger equation. Now both the wave function $\psi^{(B)}$ in the bulk and the vacuum solution $\psi^{(V)}$ are inserted into Eq. (4) (with $S_{E,\mathbf{k}_{||}}$ set to be the scattering matrix $S^c_{E,\mathbf{k}_{||}}$ of the composite structure); a tedious but straightforward calculation leads to a system of linear equations involving only the boundary value $c^{(V)}_R := (\Lambda - \partial_z)\psi^{(V)}|_{z_V}$ and the coefficients $\underline{\alpha}_+ := (\alpha_1, \alpha_2, \ldots, \alpha_\sigma)$ of those Bloch waves which propagate into the bulk region:

$$M_{E,\mathbf{k}_{||}} c^{(V)}_R = N_{E,\mathbf{k}_{||}} \underline{\alpha}_+ . \tag{8}$$

For the sake of brevity, explicit formulas for $M_{E,\mathbf{k}_{||}}$ and $N_{E,\mathbf{k}_{||}}$ are omitted here. However, it should be noted that these operators can be completely expressed in terms of the coefficients $\mathscr{R}$ and $\mathscr{T}$ of $S^c_{E,\mathbf{k}_{||}}$ and those $2\sigma(E,\mathbf{k}_{||})$ solutions to the eigenvalue problem (5) which are related to the real band structure. Thus, any numerical problems arising from the exponentially decaying evanescent waves are excluded.

Both scattering states and bound states are determined by (8), but only the latter shall be discussed here. In this case, the operator $M_{E,\mathbf{k}_{||}}$ is injective and hereby invertible [except for discrete values of $E = E^{ss}_j(\mathbf{k}_{||})$; $j = 1,2,3,\ldots$]; hence, by inversion of $M_{E,\mathbf{k}_{||}}$, the general solution $c^{(V)}_R$ to (8) is obtained in terms of the coefficients $\underline{\alpha}_+$ yielding a complete characterization of the $\sigma(E,\mathbf{k}_{||})$-dimensional space of "surface-adapted bulk states." Of course, if $\sigma(E,\mathbf{k}_{||}) = 0$ (i.e., within an absolute band gap), bound states of this kind do not exist. Nevertheless, if in this situation E equals one of the values $E^{ss}_j(\mathbf{k}_{||})$, a nontrivial solution $c^{(V)}_R$ to (8) exists, although the right-hand side vanishes. This is characteristic of a surface state, since according to (6) the probability density of the electron is negligible in the deep bulk. In practice, the classification of the solutions to (8) is most appropriately performed by a (numerical) singular value decomposition[35,36] of the operator $M_{E,\mathbf{k}_{||}}$: Let $\kappa_{\min}(E,\mathbf{k}_{||})$ denote the smallest singular value of $M_{E,\mathbf{k}_{||}}$; then a peak pointing downwards to and situated at the E axis denotes a surface state [see Fig. 2(a)], whereas a smooth behavior of $\kappa_{\min}$ above the E

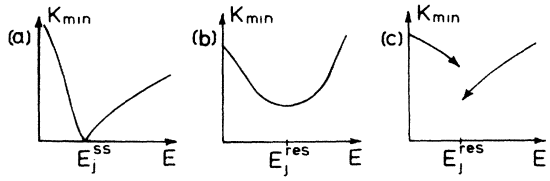

FIG. 2. Behavior of the smallest singular value $\kappa_{\min}(E)$ of the "matching matrix" $\underline{M}^{PW}$ in the neighborhood of a surface state (a) or a surface resonance (b), (c).

axis indicates surface-adapted bulk states [provided that $\sigma(E,\mathbf{k}_{||})>0$ holds]. An interesting case occurs if $\kappa_{\min}(E,\mathbf{k}_{||})$ exhibits a minimum close to the E axis, but without tangency. In this situation, the operator $M_{E,\mathbf{k}_{||}}$ may be regarded as being "nearly singular," i.e., the amplitudes $\underline{\alpha}$ of the wave function deep in the crystal do not vanish, but they are small compared to the amplitude of the singular vector belonging to $\kappa_{\min}$, which dominates in the surface region. Usually this phenomenon is called a "surface resonance." Lastly, as a delicate case, $\kappa_{\min}(E,\mathbf{k}_{||})$ may happen to have a zero where $\sigma(E,\mathbf{k}_{||})>0$ holds. If this occurs within a relative band gap, and if the singular vector related to $\kappa_{\min}=0$ differs in symmetry from all the $2\sigma(E,\mathbf{k}_{||})$ propagating waves, it makes sense to speak of a "relative surface state" (in contrast to an "absolute surface state" situated within an absolute band gap as discussed above); otherwise, if no distinction by symmetry is possible, only a mixture of the singular vector localized at the surface and the propagating waves in the bulk can be detected by a physical experiment. Hence, the notion of a surface resonance is appropriate to this situation. Since relative band gaps are confined to symmetry lines in $\mathbf{k}_{||}$ space, it depends on the $\mathbf{k}_{||}$ resolution of an experiment and the kind of $\mathbf{k}_{||}$-averaging processes involved in it, whether or not it is reasonable to differentiate between relative surface states and resonances.[37,38]

III. NUMERICAL REALIZATION

As the ABCM method has been formulated without reference to a special basis of trial functions, one is yet free to choose the type of numerical discretization. Among various discretization methods applicable to the monolayer problem, an augmented-plane-wave-like[39,40] method is presented here. Starting from an equivalent variational problem[41] (suitable even for discontinuous trial functions) and assuming a warped muffin-tin form of the potential

$$w(\mathbf{r})=\begin{cases} V_{\text{sph}}(|\mathbf{r}_j|) & \text{if } |\mathbf{r}_j|:=|\mathbf{r}-\tau_j|\le s_j\ , \\ V(\mathbf{r}) & \text{elsewhere} \end{cases} \tag{9}$$

(τ_j and s_j denote center and radius of the jth muffin-tin sphere), the following ansatz for the trial functions is made. Inside a muffin-tin sphere an angular momentum representation is used:

$$\varphi(\mathbf{r})=\sum_{l=0}^{L}\sum_{|m|\le l} A_{lm}R_l(E,r_j)Y_{lm}(\hat{\mathbf{r}}_j) \tag{10}$$

[$R_l(E,r)$ is the solution to the radial Schrödinger equation for angular momentum l; $Y_{lm}=$ spherical harmonics]. In the region outside the muffin-tin spheres the wave function is approximated by a planar Fourier series

$$\varphi(\mathbf{r})=\sum_{n=0}^{N}\sum_{\mathbf{g}} B_{n\mathbf{g}}T_n(\xi)e^{i(\mathbf{k}_{||}+\mathbf{g})\cdot\mathbf{r}_{||}}\ . \tag{11}$$

Here, T_n are the Chebyshev polynomials[42] and ξ is a scaled coordinate defined by $z=z_L+(1+\xi)d/2$. There are several arguments why an expansion of this form is favorable: First, those matrix elements of the discrete Schrödinger equation which do not depend on the potential $w(\mathbf{r})$ are easy to evaluate by means of well-known functions. Second, with respect to the potential-dependent matrix elements, numerical integration is facilitated by the use of a Gauss-type integration rule which combines both a high rate of convergence and the advantage of equidistant nodes. Furthermore, the discretization error introduced by the truncated Chebyshev expansion (11) is directly controlled by the coefficients $B_{n\mathbf{g}}$.[43] Lastly, the identity

$$2T_n(\xi)T_m(\xi)=T_{m+n}(\xi)+T_{|n-m|}(\xi) \tag{12}$$

permits economizing computer storage, since the number of different matrix elements per $\mathbf{g}$ vector amounts only to $2N+1$ instead of the usual number $(N+1)(N+2)/2$.

The stationary points of the variational expression are now determined by the system of linear equations

$$\sum_{p,\mathbf{g}'}\hat{M}_{n\mathbf{g},p\mathbf{g}'}B_{p\mathbf{g}'}=b_{\mathbf{g}}^{R}+(-1)^n b_{\mathbf{g}}^{L}\ , \tag{13}$$

where $b_{\mathbf{g}}^{R}$ and $b_{\mathbf{g}}^{L}$ denote the planar Fourier coefficients of the boundary data (1). For the sake of simplicity, let us only treat the case of a single atom basis; then the matrix $\hat{\underline{M}}$ is given as the sum of Hermitian matrices

$$\hat{\underline{M}}=\underline{M}^{(1)}+\underline{M}^{(0)}+\underline{\Lambda}+\sum_{l=0}^{L}\frac{r_0^2}{A}(r_0L_l-\rho)\underline{\mathscr{S}}^{(l)} \tag{14}$$

(r_0 is the muffin-tin radius; A is the unit area in the $\mathbf{r}_{||}$ plane), which are defined as follows: Let

$$(f\,|\,g):=\int_{-1}^{1}f^*(\xi)g(\xi)d\xi \tag{15}$$

denote the inner product of $L_2(-1,1)$ functions; then

$$\begin{aligned} M^{(i)}_{n\mathbf{g},p\mathbf{g}'}:=[(\mathbf{k}_{||}+\mathbf{g})\cdot(\mathbf{k}_{||}+\mathbf{g}')r_0^2-Er_0^2]^{1-i}\times\Bigg[&\delta_{\mathbf{g}\mathbf{g}'}\left[(T_n^{(i)}\,|\,T_p^{(i)})-\frac{r_0^2\pi}{A}(T_n^{(i)}\,|\,(1-\xi^2)\,|\,T_p^{(i)})\right] \\ &-(1-\delta_{\mathbf{g}\mathbf{g}'})\frac{r_0^2\pi}{A}\frac{2}{|\mathbf{g}-\mathbf{g}'|r_0}\mathscr{M}^{(i)}_{np}(|\mathbf{g}-\mathbf{g}'|r_0)\Bigg] \\ &+(1-i)\left[\rho\times 2\frac{r_0^2\pi}{A}\mathscr{N}_{np}(|\mathbf{g}-\mathbf{g}'|r_0)+\mathscr{W}_{n\mathbf{g},p\mathbf{g}'}\right], \end{aligned} \tag{16}$$

where

$$\mathscr{M}^{(i)}_{np}(\gamma) := (T^{(i)}_n \mid (1-\xi^2)^{1/2} J_1(\gamma(1-\xi^2)^{1/2}) \mid T^{(i)}_p) , \quad (17)$$

$$\mathscr{N}_{np}(\gamma) := (T_n \mid J_0(\gamma(1-\xi^2)^{1/2}) \mid T_p) \quad (18)$$

[$J_m(x)$ is the Bessel function of the first kind and of order m]. $\mathscr{W}_{ng,pg'}$ denotes a term dependent on the potential $w(\mathbf{r})$, which will be discussed below. Furthermore, it is defined

$$\Lambda_{ng,pg'} := \alpha[\,|\mathbf{k}_{||}+\mathbf{g}|^2+E_0(\mathbf{k}_{||})]^{1/2} r_0[1+(-1)^{n+p}]\delta_{gg'} \quad (19)$$

[α and $E_0(\mathbf{k}_{||})$ being positive numerical parameters] and

$$\mathscr{S}^{(l)}_{ng,pg'} := \sum_{\substack{m \\ |m| \le l}} \mathscr{K}_{lm,ng} \times \mathscr{K}_{lm,pg'} , \quad (20)$$

$$\mathscr{K}_{lm,ng} := [1+(-1)^{l+m+n}] N^m_l c_m(\mathbf{g}) \times \mathscr{P}_{lmn}(\,|\mathbf{k}_{||}+\mathbf{g}|\, r_0) , \quad (21)$$

where

$$N^m_l := \left[\frac{2l+1}{2}\frac{(l-m)!}{(l+m)!}\right]^{1/2} , \quad (22)$$

$$\mathscr{P}_{lmn}(\gamma) := \int_0^1 P^m_l(\xi) J_m(\gamma(1-\xi^2)^{1/2}) T_n(\xi) d\xi . \quad (23)$$

The coefficients $c_m(\mathbf{g})$ depend on the azimuth of

$$\mathbf{k}_{||}+\mathbf{g} = |\mathbf{k}_{||}+\mathbf{g}|\,[-\sin(\vartheta_g)\mathbf{e}_x + \cos(\vartheta_g)\mathbf{e}_y]$$

by

$$c_m(\mathbf{g}) := \begin{cases} \sqrt{2\pi}, & m=0 , \\ 2\sqrt{\pi}\cos[m\vartheta(\mathbf{g})], & m \ge 1 , \\ 2\sqrt{\pi}\sin[\,|m|\,\vartheta(\mathbf{g})], & m \le -1 . \end{cases} \quad (24)$$

L_l denotes the logarithmic derivative of the radial function R_l at $r=r_0$. The parameters ρ, α, and E_0 have no physical significance, but they may be used to control convergence and accuracy.[15,41] It should be noted that the coefficients A_{lm} in the L representation (10) have already been eliminated in Eq. (13); if desired, they are obtained by

$$A_{lm} R_l(E,r_0) = \sum_{n,g} \mathscr{K}_{lm,ng} B_{ng} . \quad (25)$$

All integrals appearing from (16) to (23) are analytically evaluated by means of standard tables[44] and implemented in the computer program using standard routines for the "special functions."[45,46]

Besides the logarithmic derivatives L_l, the matrix elements $\mathscr{W}_{ng,pg'}$ contain all information about the potential $w(\mathbf{r})$; they are defined as

$$\mathscr{W}_{ng,pg'} := \frac{r_0^2}{A}(T_n \mid \Delta V(\mathbf{g},\mathbf{g}',\xi) \mid T_p) , \quad (26)$$

with $\Delta V(\mathbf{g},\mathbf{g}',\xi) = V^{PW}(\mathbf{g}-\mathbf{g}',\xi) - V^B(\,|\mathbf{g}-\mathbf{g}'|\,,\xi)$, where

$$V^{PW}(\mathbf{g},\xi) := \int_Z w(\mathbf{r}_{||}, r_0\xi) e^{-i\mathbf{g}\cdot\mathbf{r}_{||}} d^2 r_{||} , \quad (27)$$

$$V^B(g,\xi) := \int_0^{r_0(1-\xi^2)^{1/2}} V_{\mathrm{sph}}([\rho^2+(r_0\xi)^2]^{1/2}) \times 2\pi J_0(g\rho)\rho\, d\rho . \quad (28)$$

Because of (12), the numerical integration of (26) involves only integrals of the form $(T_p \mid \Delta V(\mathbf{g},\mathbf{g}',\cdot))$ for $p=0,1,\ldots,2N$. Here, the following (Gauss-type) integration rule proved to be very efficient: Let us decompose

$$(T_p \mid f) = f(1)\times 2\times(1-p^2)^{-1}\hat{\delta}_p + (T_p \mid \tilde{f}) , \quad (29)$$

with $\tilde{f}(\xi) := f(\xi)-f(1)$, $\hat{\delta}_p := \frac{1}{2}[1+(-1)^p]$; then $(T_p \mid \tilde{f})$ is approximated by

$$(T_p \mid \tilde{f}) \approx T_p^{(M)}(\tilde{f}) := \frac{\pi}{2M+1} \sum_{j=0}^{2M} \sin(\theta_j)\cos(p\theta_j) \times \tilde{f}(\cos(\theta_j)) , \quad (30)$$

where the (equidistant!) nodes θ_j are given by

$$\theta_j := \frac{\pi}{4M+2}(2j+1), \quad j=0,1,\ldots,2M . \quad (31)$$

It is worth mentioning that the residual term in (30) can be calculated by means of the Chebyshev coefficients of $\tilde{f}$,[47] thus providing an *a priori* estimate quite useful in practice. For the numerical evaluation of the integrals $\Delta V(\mathbf{g},\mathbf{g}',\xi_j)$ at the nodes $\xi_j=\cos(\theta_j)$, one of those methods is to be favored which is especially adapted to the translational symmetry of the integrands.[48-52]

Solving the linear system (13) with the right-hand side chosen as $b^\sigma_g := \delta_{gg'}\delta_{\sigma\sigma'}$ yields coefficients $B^{g'\sigma'}_{ng}$ which are used to calculate the planar Fourier representation of the monolayer scattering matrix according to

$$\mathscr{R}_X = 2\hat{\underline{\Lambda}}\underline{G}_{XX}, \quad \mathscr{T}_{XY} = 2\hat{\underline{\Lambda}}\underline{G}_{XY} \quad (X,Y=R,L) , \quad (32)$$

where $\hat{\underline{\Lambda}}$ is diagonal with matrix elements $\hat{\Lambda}_g = \frac{1}{2}\Lambda_{0g,0g}$, and $\underline{G}_{XY}$ has the matrix elements

$$G_{RR}(\mathbf{g},\mathbf{g}') = \sum_{n=0}^{N} B^{g'R}_{ng}, \quad G_{RL}(\mathbf{g},\mathbf{g}') = \sum_{n=0}^{N} B^{g'L}_{ng} ,$$
$$G_{LR}(\mathbf{g},\mathbf{g}') = \sum_{n=0}^{N} (-1)^n B^{g'R}_{ng}, \quad G_{LL}(\mathbf{g},\mathbf{g}') = \sum_{n=0}^{N} (-1)^n B^{g'L}_{ng} . \quad (33)$$

The discrete form of (5) then reads

$$\underline{e}(\mathbf{a}_{3||}) \oplus \underline{e}(\mathbf{a}_{3||}) \begin{bmatrix} \mathscr{R}_R - \underline{1} & \mathscr{T}_{RL} \\ \underline{1} & \underline{0} \end{bmatrix} \begin{bmatrix} \underline{b}_R \\ \underline{b}_L \end{bmatrix} = t_\perp \begin{bmatrix} \underline{0} & \underline{1} \\ \mathscr{T}_{LR} & \mathscr{R}_L - \underline{1} \end{bmatrix} \begin{bmatrix} \underline{b}_R \\ \underline{b}_L \end{bmatrix} , \quad (34)$$

with $\underline{e}(\mathbf{a}_{3\|})$ being a diagonal matrix with the elements $\exp(i\mathbf{g}\cdot\mathbf{a}_{3\|})$; the eigenvalue $t_\perp$ equals $\exp(ik_\perp d)$. For basic mathematical reasons the matrices at both sides of (34) are ill conditioned; thus, the application of the QZ algorithm[53–56] is favorable, since it has been designed exactly for this situation.

After calculating the $\sigma(E,\mathbf{k}_\|)$ propagating Bloch waves $(\underline{\mathbf{b}}_R^{(\mu)},\underline{\mathbf{b}}_L^{(\mu)})$ from (34) which are traveling into the bulk region, the layer-doubling process is performed in the following way: Let $\underline{\mathscr{R}}_X^{(n)}$ and $\underline{\mathscr{T}}_{XY}^{(n)}$ [or $\underline{G}_{XY}^{(n)}$ according to (32), respectively] denote the coefficients of the bulk scattering matrix after the nth reduplication operation, and let $\underline{Q}_p^{(n)}$ denote the orthogonal projector on the linear space spanned by the vectors

$$\underline{\mathbf{s}}_n^{(\mu)} := i\underline{G}_{LR}^{(n)}\underline{\mathbf{b}}_R^{(\mu)} \quad [\mu=1,2,\ldots,\sigma(E,\mathbf{k}_\|)] \ . \tag{35}$$

Then, layer doubling is terminated, if

$$||\underline{Q}_p^{(n+1)}-\underline{Q}_p^{(n)}|| < \varepsilon(Q)$$

and

$$||\underline{\mathscr{R}}_L^{(n+1)}\underline{Q}_{ev}^{(n+1)}-\underline{\mathscr{R}}_L^{(n)}\underline{Q}_{ev}^{(n)}|| < \varepsilon(\mathscr{R}) \tag{36}$$

(with $\underline{Q}_{ev}^{(n)} := \underline{1}-\underline{Q}_p^{(n)}$) is satisfied with $\varepsilon(Q)$ and $\varepsilon(\mathscr{R})$ being chosen sufficiently small. Of course, if $\sigma(E,\mathbf{k}_\|)=0$, then $\underline{Q}_p^{(n)}=\underline{0}$ and $\underline{Q}_{ev}^{(n)}=\underline{1}$ must be set in (36). It has been shown[15] that the layer-doubling process converges as $(t_{ev})^{2^n}$, where

$$t_{ev} := \max\{e^{-|\mathrm{Im}k_\perp^{(\nu)}|d}; |t_\perp^{(\nu)}|\neq 1\} \ . \tag{37}$$

Hence, that real line of the complex band structure, which is situated next to the bulk band structure (at the given energy E), determines the rate of convergence. Especially, the closer E approaches a band edge, the worse the layer doubling will converge. In order to achieve an accuracy of D digits, the number n of layer reduplications amounts to

$$n \approx \log_{10}[-D/\log_{10}t_{ev}]/\log_{10}(2) \ . \tag{38}$$

Finally, the discrete analog to Eq. (8) has to be set up. It is advantageous to write the planar Fourier coefficients of the wave function (7) outside the half-crystal in the equilibrated form

$$u^{(V)}(\mathbf{g},z)=\beta_{\mathbf{g}}u(\eta_{\mathbf{g}},z)/u(\eta_{\mathbf{g}},z_V) \ , \tag{39}$$

where $u(\eta_{\mathbf{g}},z)$ is obtained by numerical integration of the (one-dimensional) Schrödinger equation for $z\le z_V$, and $\beta_{\mathbf{g}}$ is to be determined from (8). For the simple case of an ideal crystal surface, the explicit form of this system of linear equations shall be given: Let

$$\underline{D}_V := \mathrm{diag}\left[r_0\frac{d}{dz}u(\eta_{\mathbf{g}},z_V)\Big/u(\eta_{\mathbf{g}},z_V)\right] \tag{40}$$

be defined as the diagonal matrix of the logarithmic derivatives of $u(\eta_{\mathbf{g}},z)$ at $z=z_V$, and let

$$\underline{b}_L := (\underline{\mathbf{b}}_L^{(1)},\underline{\mathbf{b}}_L^{(2)},\ldots,\underline{\mathbf{b}}_L^{(2\sigma)}) \ , \tag{41}$$

$$\underline{b}_R := \underline{e}(\mathbf{a}_{3\|})(t_\perp^{(1)*}\underline{\mathbf{b}}_R^{(1)},t_\perp^{(2)*}\underline{\mathbf{b}}_R^{(2)},\ldots,t_\perp^{(2\sigma)*}\underline{\mathbf{b}}_R^{(2\sigma)}) \tag{42}$$

be built up by the "left" and "right" components of the $2\sigma(E,\mathbf{k}_\|)$ propagating solutions to (34), and let

$$\underline{E} := (\underline{\mathbf{e}}_1,\underline{\mathbf{e}}_2,\ldots,\underline{\mathbf{e}}_\sigma) \tag{43}$$

denote an orthonormal basis of the range of $\underline{Q}_p^{(n)}$ (i.e., $\underline{Q}_p^{(n)}=\sum_{\mu=1}^{\sigma}\underline{e}_\mu\underline{e}_\mu^\dagger$). Then, the coefficients $\underline{\boldsymbol{\beta}}=(\beta_{\mathbf{g}})$ characterizing the vacuum solution (7) and $\underline{\boldsymbol{\alpha}}=(\alpha_1,\alpha_2,\ldots,\alpha_{2\sigma})$ characterizing the bulk solution (6) satisfy the system of equations

$$\underline{M}^{\mathrm{PW}}\underline{\boldsymbol{\beta}}-\underline{N}^{\mathrm{PW}}\underline{\boldsymbol{\alpha}}=\underline{0} \ , \tag{44}$$

where

$$\underline{M}^{\mathrm{PW}} := \begin{bmatrix} \underline{\mathscr{R}}_L\underline{Q}_{ev}(\hat{\underline{\Lambda}}-\underline{D}_V)-2\hat{\underline{\Lambda}} \\ \underline{E}^\dagger(\hat{\underline{\Lambda}}-\underline{D}_V) \end{bmatrix} , \tag{45}$$

$$\underline{N}^{\mathrm{PW}} := \begin{bmatrix} (\underline{\mathscr{R}}_L\underline{Q}_{ev}-\underline{1})\underline{b}_L-\underline{b}_R \\ \underline{E}^\dagger\underline{b}_L \end{bmatrix} . \tag{46}$$

Let N_G be the number of $\mathbf{g}$-vectors included in (11); then, the linear system (44) consists of $N_G+\sigma$ equations for the $N_G+2\sigma$ unknown variables $\underline{\boldsymbol{\beta}}$ and $\underline{\boldsymbol{\alpha}}$. Hence, it defines the σ-dimensional space of surface-adapted bulk states, provided that both $\underline{M}^{\mathrm{PW}}$ and $\underline{N}^{\mathrm{PW}}$ have maximal rank (equal to the regular case). Instead of eliminating $\alpha_{\sigma+1},\alpha_{\sigma+2},\ldots,\alpha_{2\sigma}$ [this would directly lead to Eq. (8)], it is favorable for numerical reasons to proceed in the following way: First, $\underline{M}^{\mathrm{PW}}$ is factorized by a singular value decomposition[36] as

$$\underline{M}^{\mathrm{PW}}=\underline{V}\begin{bmatrix}\underline{\kappa}\\ \underline{0}\end{bmatrix}\underline{U}^\dagger \ , \tag{47}$$

where $\underline{U}$ and $\underline{V}$ are unitary matrices of dimension N_G and $N_G+\sigma$, respectively, and $\underline{\kappa}=\mathrm{diag}(\kappa_1,\kappa_2,\ldots,\kappa_{N_G})$ is the diagonal matrix of singular values $\kappa_1\ge\kappa_2\ge\cdots\ge\kappa_{N_G}\ge 0$. Thus, in the regular case, Eq. (44) can be solved for $\underline{\boldsymbol{\beta}}$ in the form

$$\underline{\boldsymbol{\beta}}=\underline{U}\underline{\kappa}^{-1}\underline{V}_1^\dagger\underline{N}^{\mathrm{PW}}\underline{\boldsymbol{\alpha}}, \ \text{if} \ \underline{V}_2^\dagger\underline{N}^{\mathrm{PW}}\underline{\boldsymbol{\alpha}}=\underline{0} \ . \tag{48}$$

Here,

$$\underline{V}_1 := (\underline{\mathbf{v}}_1,\underline{\mathbf{v}}_2,\ldots,\underline{\mathbf{v}}_{N_G})$$

and

$$\underline{V}_2 := (\underline{\mathbf{v}}_{N_G+1},\underline{\mathbf{v}}_{N_G+2},\ldots,\underline{\mathbf{v}}_{N_G+\sigma})$$

consist of the N_G, first, and the σ, last, columns of $\underline{V}$. Performing a further singular-value decomposition

$$\underline{V}_2^\dagger\underline{N}^{\mathrm{PW}}=\underline{Z}(\underline{\delta},\underline{0})\underline{W}^\dagger \tag{49}$$

(with $\underline{W}$ and $\underline{Z}$ being unitary matrices of dimension 2σ and σ, respectively, and $\underline{\delta}$ being the diagonal matrix of singular values $\delta_1,\delta_2,\ldots,\delta_\sigma$) yields an orthonormal set of σ vectors $\underline{\mathbf{w}}_{\sigma+1},\underline{\mathbf{w}}_{\sigma+2},\ldots,\underline{\mathbf{w}}_{2\sigma}$ (being the right half of the columns of $\underline{W}$), which span the kernel of $\underline{V}_2^\dagger\underline{N}^{\mathrm{PW}}$. Hence, the coefficients $\underline{\boldsymbol{\alpha}}$ of any surface-adapted bulk state are to be expressed as a linear combination of $\underline{\mathbf{w}}_{\sigma+1},\underline{\mathbf{w}}_{\sigma+2},\ldots,\underline{\mathbf{w}}_{2\sigma}$.

Furthermore, the singular value decomposition (47) provides a practical criterion for the existence of surface

states: Since $\underline{\alpha}=\underline{0}$ is required in this case, a surface state exists if, and only if, at least one of the singular values κ_j of $\underline{M}^{\mathrm{PW}}$ equals zero. A nontrivial solution $\underline{\beta}$ to Eq. (44) is given by the jth column $\underline{u}_j$ of the unitary matrix $\underline{U}$ in (47); if several κ_j happen to vanish simultaneously, $\underline{\beta}$ is a linear combination of the respective singular vectors $\underline{u}_j$.

In the case that the smallest singular value $\kappa_{\min}=\kappa_{N_G}$ shows a variation with energy such that a minimum close to zero occurs, the term

$$\underline{\beta}_{\mathrm{res}}=\kappa_{\min}^{-1}\underline{u}_{N_G}\underline{v}_{N_G}^{\dagger}\underline{N}^{\mathrm{PW}}\underline{\alpha} \tag{50}$$

dominates on the right-hand side of Eq. (48). Due to the small denominator $\kappa_{\min}$, the amplitude of the wave function in the surface region is distinctly enhanced in comparison with the bulk amplitude, which is the characteristic of a surface resonance. It should be noted that—in contrast to other methods[3,9,18,57,4]—there is no numerical difficulty in distinguishing a surface state from a resonance, because the qualitative behavior of $\kappa_{\min}(E)$ in the neighborhood of the energy E_j^{ss} of a surface state can be expressed as

$$\kappa_{\min}(E)=|\lambda(E)|\ , \tag{51}$$

with $\lambda(E)$ being a smooth function of energy, whereas $\kappa_{\min}(E)$ is either parabolic or discontinuous[58] near the energy E_j^{res} of a resonance (see Fig. 2).

IV. NUMERICAL RESULTS FOR Al AND Cu

The numerical calculations presented in this section should mainly serve the purpose of demonstrating the performance of the ABCM method on well-known examples, providing hereby the comparison with other methods. Therefore, the simple model of an ideal half-crystal is considered (without giving regards to any effects characteristic of a real physical surface). The use of "standard potentials," which are the basis for previous calculations of other authors, enables a direct quantitative comparison, and does not essentially restrict the possibility of verifying results concerning convergence and stability, which have been obtained by abstract mathematical reasoning.

In the bulk region, the potentials suggested by Snow[59] (for Al) and by Chodorow[60] and Burdick[61] (for Cu) were chosen. These potentials proved to be quite useful in giving both a qualitative interpretation and a quantitative explanation of the electronic properties of the surface and of the bulk.[62–64,18,65–75] Especially the Burdick potential has been revalued by the fact that the resulting theoretical energy bands are in good agreement with those obtained by photoemission or inverse-photoemission experiments;[76–79] it seems to be superior, even to self-consistently calculated potentials.[80,81]

The transition region between surface and vacuum was simulated by the analytical model potential

$$V(z)=V_0+(V_{\mathrm{vac}}-V_0)\tanh[(\pi/L)(z_w-z)]\ . \tag{52}$$

The position z_w and the width $2L$ of the surface barrier were considered as adjustable parameters, whereas the vacuum level V_{vac} was determined by experimental data of the work function $\Phi=V_{\mathrm{vac}}-E_F$.[73,82] The constant V_0 was fixed by the requirement that $V(z)$ should smoothly match the muffin-tin floor across the plane $z=z_V$. With the jellium model[83] as orientation, a potential of the form (52) seems quite reasonable; it proved to give satisfactory results in the work of other authors.[38,84]

Some tests were made in order to investigate what numerical accuracy can be achieved by increasing the number of trial functions [in (10) and (11)] and by varying the numerical parameters α and E_0 [in (19)] and ρ [in (14) and (16)]. First, all effects due to the crystal potential were turned off by setting $w(\mathbf{r})=0$ ("empty-lattice test"). The matrices $\underline{\hat{M}}$ and $\underline{G}_{XY}$ as well as the complex band structure $k_{\perp}^{(\mu)}(E,\mathbf{k}_{||})$ were numerically calculated and compared to their exact values obtained by evaluating the respective analytical expressions. It turned out that a six-digit accuracy of the real band structure requires $N\approx 17$–20 in the Chebyshev expansion (11) and about $L=10$ in the L representation (10); this agrees with the values typical of the APW method.[40,85] Since the exact matrices $\underline{G}_{XY}$ are diagonal in this special case, the number of planar Fourier coefficients in (11) does not influence the accuracy, provided all $\mathbf{g}$ vectors are regarded which span the free-electron energy bands at the given energy E. Thus, the empty-lattice test is a specific criterion for the convergence of the Chebyshev series and the expansion in spherical harmonics. The rate of convergence of the latter is influenced by the choice of the parameter ρ; setting

$$\rho=r_0 L_{L+1}(E,r_0) \tag{53}$$

proved optimal, because in this case the l summation in (14) can be considered to extend to the upper limit $L+1$ instead of L. The choice of α and E_0 [characterizing the boundary operator Λ; see (19)] is not critical, provided Λ is positive. Varying α from 0.5 to 2.0 and E_0 from 0.01 to 1 Ry yielded identical results of the complex band structure.

The above statements proved to be also true in the numerical investigation of Al and Cu, except for the fact that now the convergence of the planar Fourier series is crucial. An estimate of the accuracy of the matrices $\underline{G}_{XY}$ and the complex band structure was obtained on the one hand by increasing the number N_G of planar Fourier coefficients, and on the other hand by comparison with the real band structures calculated by Snow[59,86] and Burdick.[61] The results confirmed the author's analysis[15] according to which an accuracy of D digits of the real lines of the complex band structure is ensured within a "bell-shaped" region extending above the complex $k_{\perp}$ plane in $(k_{\perp},E)$ space ("bell of confidence"):

$$(\mathrm{Im}k_{\perp})^2\le g_{\max}^2-E-c(D)\ . \tag{54}$$

Here, $g_{\max}$ denotes the maximal length of the $\mathbf{g}$ vectors; the constant $c(D)$ increases with the number of digits desired. Furthermore, it was verified that the rate of convergence of the Fourier series strongly depends on the interlayer distance d: Completing the arguments of Tong and Van Hove,[87] it has been shown by the author that the ratio $(N_G)_{\mathrm{I}}/(N_G)_{\mathrm{II}}$ of the (minimal) numbers of $\mathbf{g}$ vectors necessary to obtain equal accuracy for two surfaces, I and

II, with different interlayer distance d_I and d_{II}, respectively, is given by

$$(N_G)_I/(N_G)_{II}=(d_{II}/d_I)^{\beta} . \quad (55)$$

An optimistic and a pessimistic estimate yield $\beta=1$ and $\beta=3$, respectively; numerical values for a fcc lattice are shown in Table I. Indeed, covering an energy range up to 3 Ry above the Fermi level with an accuracy of 1 mRy (with respect to the real band structure) required $N_G=25-29$ for Al(100) and $N_G=43-47$ for Al(110). The Cu(100) surface needed $N_G=45-49$, whereas in the case of Cu(110), $N_G=50$ was not sufficient to achieve the required accuracy; with regard to the "geometry effect" (55), one would guess a number of at least 75–89 **g** vectors to be necessary. It is not surprising that in the case of Cu the convergence of the planar Fourier series is much slower than that of Al, because the strongly localized *d*-like wave functions of Cu in the energy range between the valence bands and the lower bands of the excited states are to be properly represented only by including a relatively large number of planar plane waves, in contrast to the "free-electron"-like wave functions and energy bands of Al.

The reliability of the method even at core-state energies was demonstrated by calculating the complex band structures of Al(100) and Cu(100) in the neighborhood of the $2s$- and $2p$-core states of Al and the $3s$ and $3p$ states of Cu, respectively, for some high-symmetric $\mathbf{k}_{||}$ points. There was no problem in obtaining the almost entirely flat real energy bands within a tolerance of 0.1 mRy; thus, the bell of confidence indeed comprehends the core-state energy range deep below the complex $k_\perp$ plane, which has been accessible only by analytical methods[31,88] up to now.

Among a number of graphical representations of the calculated complex band structures, only three representative examples can be printed here (Figs. 3–5). The energy ranges from about -2.3 to 3.5 Ry (with the muffin-tin floor being chosen as energy zero), and $k_\perp$ extends into the complex plane up to $|\mathrm{Im}k_\perp|=2.3(2\pi/a_0)$, where a_0 denotes the respective lattice constant. This limit has been chosen such that the outermost real lines exhibit about half the accuracy of the bulk band structure. The middle part of the drawings is to be identified with the real energy bands along an irreducible section of a straight line in (real) **k** space, which is perpendicular to the surface considered and contains $\mathbf{k}_{||}$. The right- and left-sided parts show real lines located on symmetry planes $\mathrm{Re}\,k_\perp=\text{const}$. Dashed lines are to be interpreted as the respective side views of those branches of the complex band structure which are not contained in one of the planes drawn.

In the low-energy range, the bulk band structures are in good agreement with those of Snow[59] and Burdick[61] (within a tolerance of 1–5 mRy); as far as results for the complex bands are available,[89,19,38] there are—at least qualitatively—no serious discrepancies. The calculations presented here provide a systematic extension to regions of relatively high and very low energies reaching far in the complex $k_\perp$ plane, with the numerical accuracy being well defined. To the author's knowledge, it is the first time that such a comprehensive survey over the system of real lines could be achieved in the case of a real metal. The calculated complex band structures indeed exhibit all the properties which have been predicted theoretically;[90,91,31,92,93] for instance, no singularities occur except for branch points of the square-root type, which delimit the width of the "complex loops."

TABLE I. Ratios of interlayer distances for the fcc lattice.

I	II	$(d_{II}/d_I)^3$	d_{II}/d_I
(110)	(111)	4.35	1.63
(110)	(100)	2.83	1.41
(100)	(111)	1.54	1.15

Compared to Al, the complex band structure of Cu shows much more structural variety in the vicinity of the Fermi energy, which is mainly due to the existence of the flat *d* bands. Among many interesting phenomena, there is, for example, the peculiar closed loop *C-D* at Cu(100)-$\bar{M}$ (Fig. 3), which is connected by the "oblique" lines *B-C* and *D-E* with the complex of Z_1 lines at the *X* point. Since the complex loops of Cu reach relatively far into the $k_\perp$ plane, surface states may be formed which rapidly decay in the bulk [$|\mathrm{Im}k_\perp| \leq (0.1-0.3)(2\pi/a_0)$].

In the case of Al, however, the energy of the *d*-like states lies high enough to yield a complex band structure very similar to that of nearly free electrons in a wide energy range around the Fermi level (Figs. 4 and 5). Due to the narrow band gaps, only small vertical complex loops occur, which do not extend very far in the $k_\perp$ plane [$|\mathrm{Im}k_\perp|=(0.01-0.05)(2\pi/a_0)$]. Hence, the surface states of Al are only weakly damped while penetrating into the bulk.

The numerical determination of surface states and resonances was performed by calculating the minimal singular value $\kappa_{\min}(E)$ of $\underline{M}^{PW}$ (see Sec. III) along an appropriately spaced mesh of energies ($\Delta E \approx 0.2-5$ mRy) within the respective absolute and relative band gaps. By identifying the symmetry of the singular vector $\underline{\beta}=\underline{u}$ belonging to $\kappa_{\min}$ [see (47)ff], an *a posteriori* classification according to the symmetry group of $\mathbf{k}_{||}$ was obtained. The influence of the potential outside the half-crystal on the location of the energy of a surface state or resonance was investigated by variation of the parameters z_w and L [see (52)]; as can be guessed from simple analytical models,[94–100] the sensitivity to the form of the vacuum potential varies very much, so the energy of the $\bar{M}_3$ state at Cu(100) (see Fig. 6) changes only within 1 mRy for $-2 \leq z_w \leq 0$ and $10^{-3} \leq L \leq \pi$ (atomic units), whereas the $\bar{\Gamma}_1$ state situated in the absolute band gap between X_4' and X_1 is shifted by nearly 100 mRy towards higher energies, when the potential barrier chosen is very steep and very close to the surface.

Assuming the arguments of the authors cited to be valid also in the general case, this may be intuitively interpreted as follows: For a surface state to exist, it is crucial that the logarithmic derivatives of the planar Fourier coefficients of the wave function have equal limits when they approach $z=z_V$ from the right and from the left. There is a good chance to satisfy this condition if either of

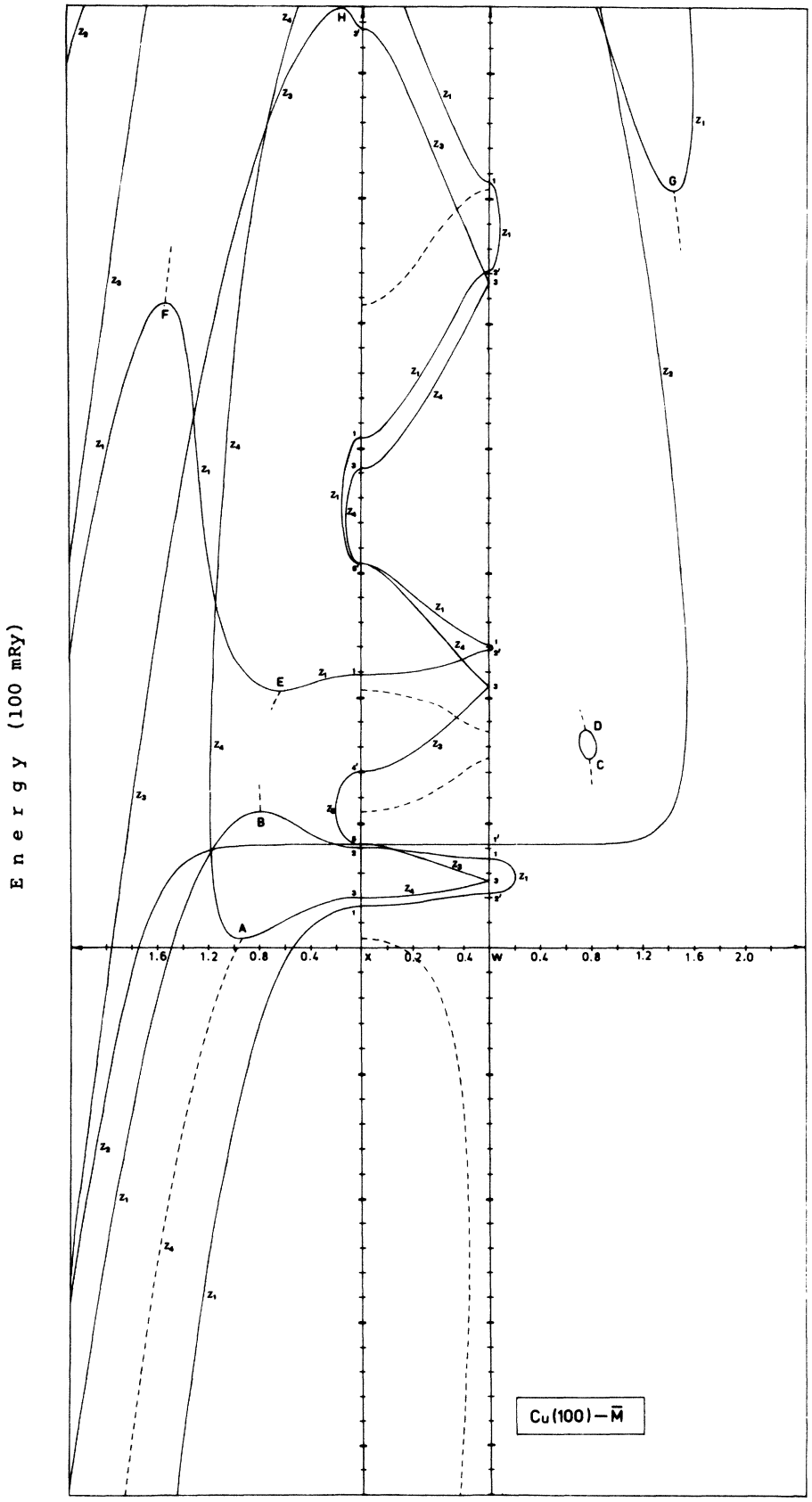

FIG. 3. Real lines of the complex band structure of Cu(100)-$\overline{M}$.

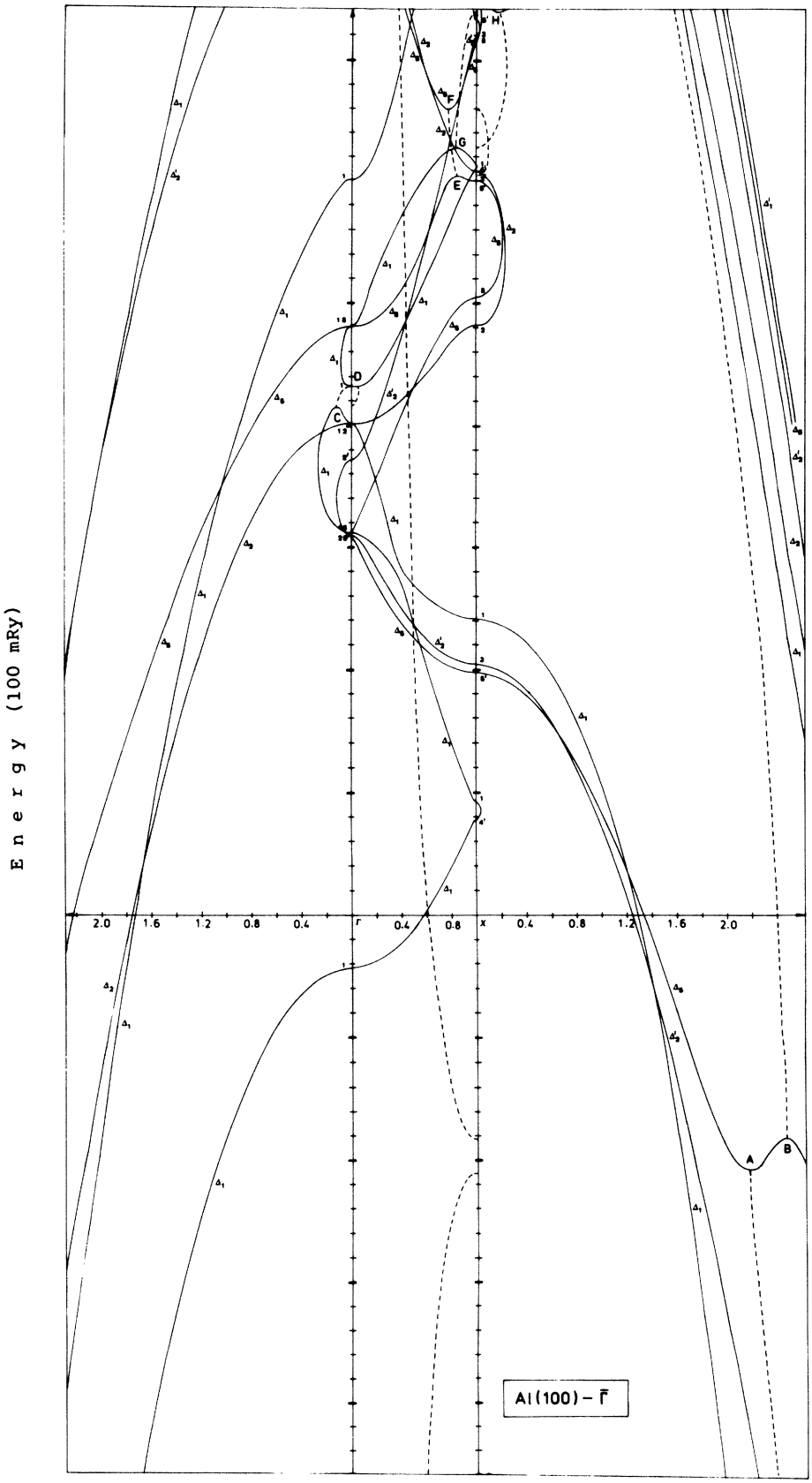

FIG. 4. Real lines of the complex band structure of Al(100)-$\bar{\Gamma}$.

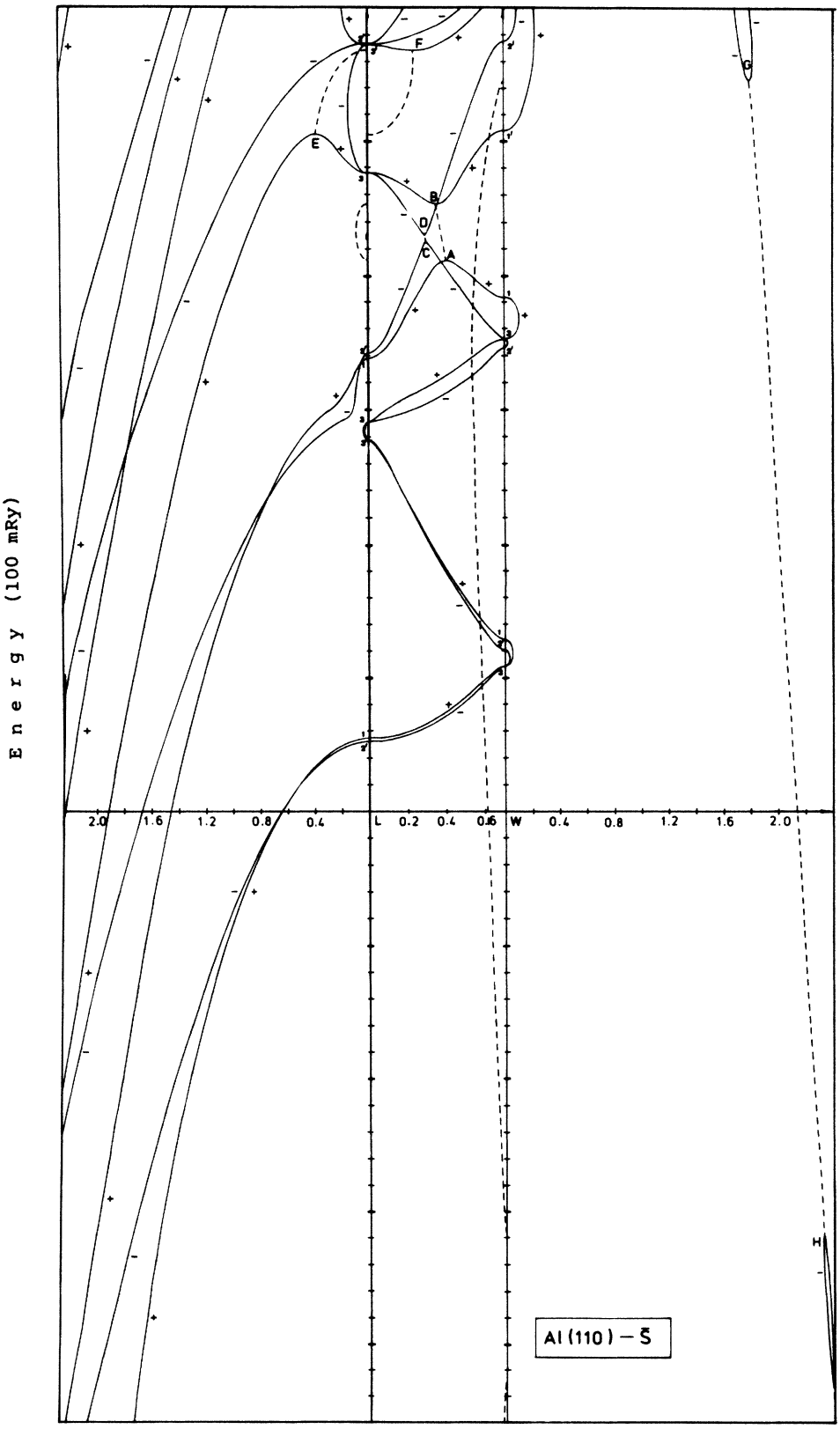

FIG. 5. Real lines of the complex band structure of Al(110)-$\bar{S}$.

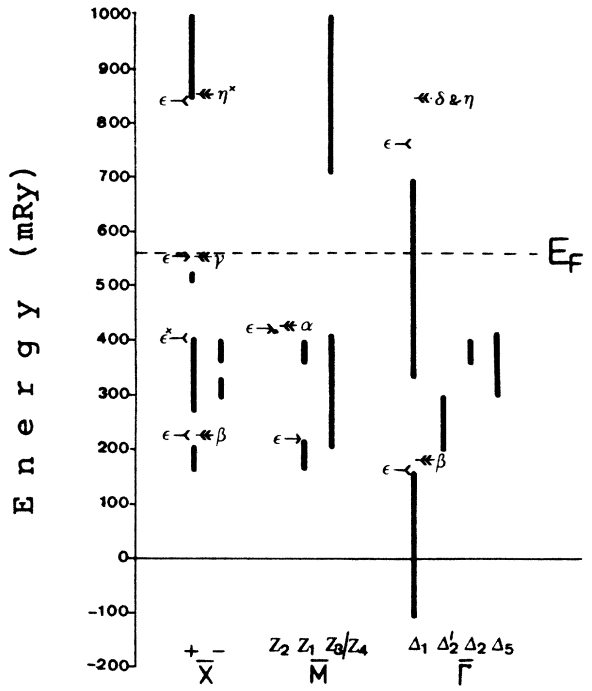

FIG. 6. Surface states of Cu(100) embedded in the symmetry-resolved projected band structure (vertical bars) at the high-symmetric $\mathbf{k}_{\|}$ points $\bar{\Gamma}$, $\bar{M}$, and $\bar{X}$. Calculated surface states are denoted by ε; when two surface symmetries are compatible with the same bulk symmetry, $\varepsilon\rightarrow$ ($\varepsilon\prec$) denotes the irreducible representation with greater (lesser) index. Experimental values: α is from Heimann *et al.* (Ref. 70), β is from Westphal and Goldmann (Ref. 73), γ is from Kevan (Ref. 105), δ is from Straub and Himpsel (Ref. 107), and η is from Dose *et al.* (Ref. 75). (Resonances are marked by $\times$.)

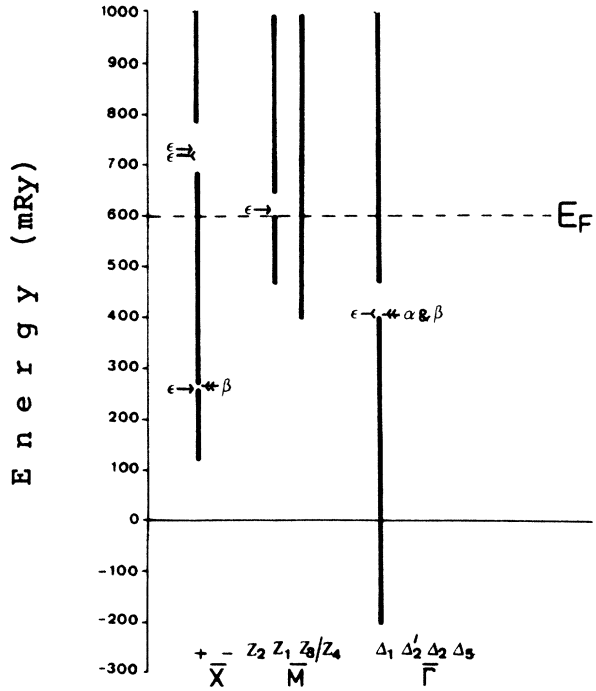

FIG. 7. Surface states of Al(100) embedded in the symmetry-resolved projected band structure (vertical bars) at the high-symmetric $\mathbf{k}_{\|}$ points $\bar{\Gamma}$, $\bar{M}$, and $\bar{X}$. Calculated surface states are denoted by ε; when two surface symmetries are compatible with the same bulk symmetry, $\varepsilon\rightarrow$ ($\varepsilon\prec$) denotes the irreducible representation with greater (lesser) index. Experimental values: α is from Gartland and Slagsvold (Ref. 65) and Hansson and Flodström (Ref. 102), and β is from Levinson *et al.* (Ref. 103).

the limits rapidly varies with energy. On the side of the half-crystal, this occurs in a (sufficiently narrow) band gap,[95,101] or in the case that a real line of the complex band structure, coming far from the interior of the $k_{\perp}$ plane joins an almost flat bulk energy band [e.g., the Z_2 band at Cu(100)-$\bar{M}$; see Fig. 3]. Thus, surface states of this kind are strongly coupled with the bulk properties of the half-crystal, and they are nearly independent of the detailed shape of the surface barrier ("crystal-induced surface states"[100]). Examples are the states $\bar{\Gamma}_1$, $\bar{X}_3$, and $\bar{M}_4$ at Al(100) (Fig. 7) and the surface states of Cu(100) below the Fermi energy (Fig. 6).

On the vacuum side, the variation of the logarithmic derivatives increases as the energy approaches the vacuum level of the potential.[100] Furthermore, at fixed energy, they are very sensitive to slight changes of z_w and L. This explains not only the existence of surface states in ranges of energy where the logarithmic derivatives of the half-crystal do not vary appreciably, but also the reason for such a strong sensitivity to the form of the vacuum potential ("barrier-induced surface states"). The $\bar{\Gamma}_1$ and $\bar{X}_1$ states at Cu(100) above the Fermi level belong to this class.

Since both occupied and unoccupied surface states of Al and Cu have been observed experimentally, it was suggestive to fit the theoretical results by an appropriate choice of z_w and L. In Figs. 6 and 7, the optimal fit of the calculated surface-state energies (at the high-symmetric $\mathbf{k}_{\|}$ points $\bar{\Gamma}$, $\bar{X}$, and $\bar{M}$) is shown in comparison with the experimental data, both being embedded in the (symmetry-resolved) projected band structure.

In the case of Al, a surface state has been measured at $\bar{\Gamma}$ about 2.75–2.80 eV below the Fermi energy, which continues in the absolute band gap extending along half the $\bar{\Gamma}$-$\bar{X}$ and the $\bar{\Gamma}$-$\bar{M}$ lines, and merges then into the energy continuum as a relative surface state or resonance.[65,102] At the $\bar{X}$ point, a surface state has been observed in the small band gap between the bulk states L_2' and L_1,[103] which disperses up towards the Fermi energy as $|\mathbf{k}_{\|}|$ decreases, and which is possibly connected with the band gap described above. Setting $z_w=0$ and $L\approx 0.5$ a.u., a $\bar{\Gamma}_1$ state about 10 mRy above the measured energy and a $\bar{X}_3$ state nearly above the band edge at L_2' were obtained. Furthermore, the calculation yielded unoccupied surface states: There are two absolute surface states, $\bar{X}_1$ and $\bar{X}_3$, about 120 and 127 mRy above E_F, respectively, and there exists a relative surface state, $\bar{M}_4$, about 10 mRy above E_F. A survey of the calculated dispersion of surface states and resonances, embedded in the projected band structure along the paths $\bar{\Gamma}$-$\bar{X}$-$\bar{M}$ and $\bar{\Gamma}$-$\bar{M}$, is displayed in Fig. 8, which represents the continuation of

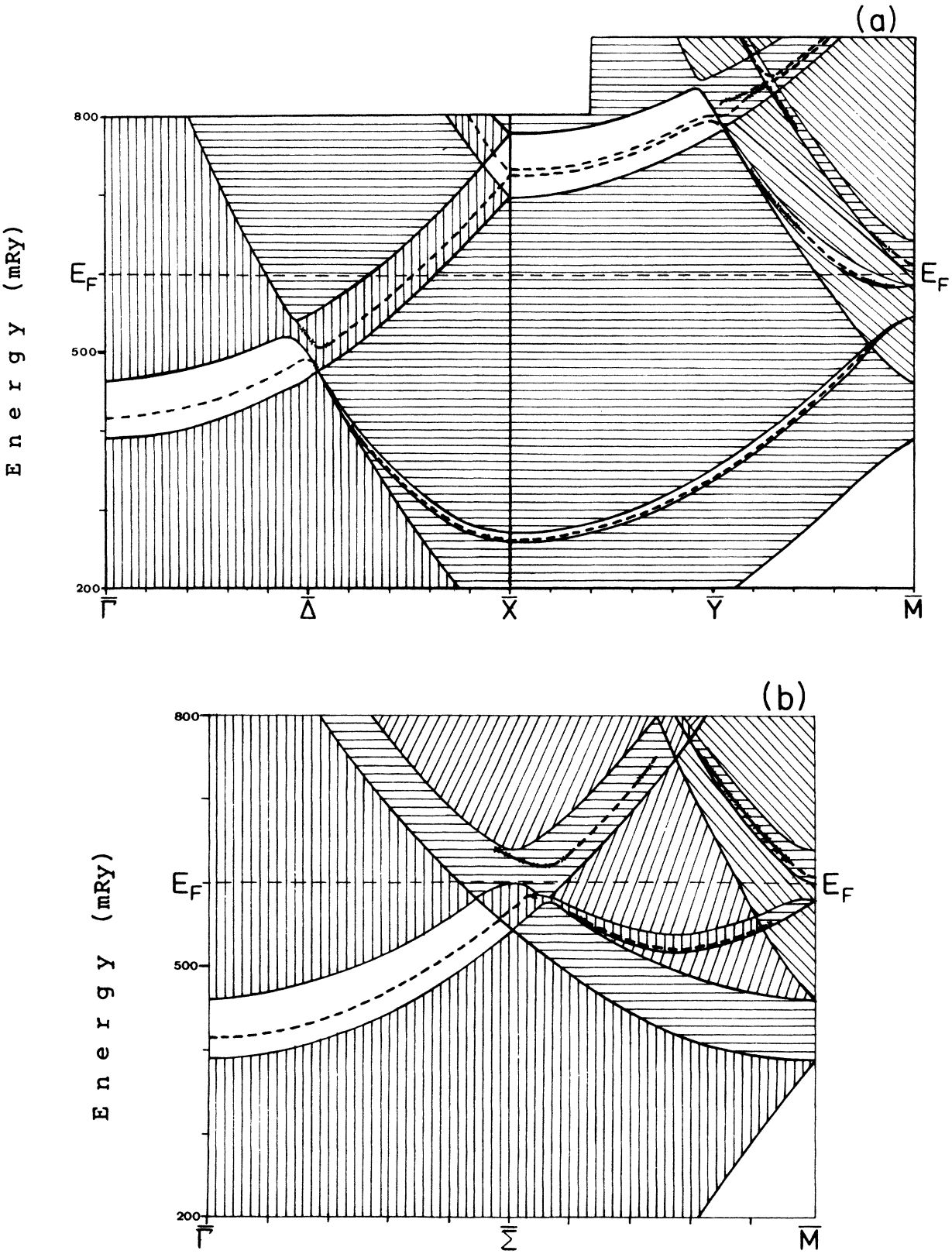

FIG. 8. Calculated dispersion of the surface states and resonances of the Al(100) surface along the paths $\bar{\Gamma}-\bar{X}-\bar{M}$ (a) and $\bar{\Gamma}-\bar{M}$ (b). The dispersion curves are embedded in the projected band structure, which is indicated by cross hatching: |||| denotes a simple, ≡ a twofold, /// a threefold, and \\\ a fourfold overlay of bulk energy bands. Both absolute and relative surface states are indicated by — — —, surface resonances by —×—×—×—.

the results of Spanjaard *et al.*[18] in three regards: First, by resolving the projected band structure according to the number $\sigma(E,\mathbf{k}_{\parallel})$ of "overlaid" bulk bands (see Sec. II), "filled band gaps" are easy to recognize. Thus, it is clarified where a surface resonance or a relative surface state is to be expected. Second, it becomes theoretically evident that an (absolute) surface state does not simply terminate at the boundary of an absolute band gap, but—generally—merges into the continuum: Since in most cases that energy band which "fills" a projected band gap is clearly separated in $\mathbf{k}$ space from the band edges which define the (relative) gap, an (absolute) surface state is likely to reappear as resonance or a relative surface state beyond the region where the projected gap is intersected by the filling band. If the symmetry of this band differs from that of the gap edges, the dispersion of the surface state is not affected at all while passing the line of intersection; otherwise, a local distortion occurs due to hybridization. Lastly, it is illustrated that generally a relative surface state or a surface resonance is allowed to exist only within a limited range in $\mathbf{k}_{\parallel}$ space. However, this range is not sharply defined; usually, a relative surface state first changes into a resonance, which then gradually disappears when approaching the boundary of a filled gap. As far as comparable, the theoretical dispersion curves agree well with experiment and, furthermore, confirm the interpretation given by the respective authors.[65,102] It should be pointed out that the agreement is indeed one-to-one, in contrast to Seel's self-consistent investigations[104] yielding additional resonances along the $\bar{\Gamma}$-$\bar{X}$ line, the interpretation of which seems rather problematic to the author.

In the case of the Cu(100) surface, a variety of surface states have been detected, which provides examples *par excellence* for each of the "classical" types as they were originally discussed in the 1930s. So, at the $\bar{\Gamma}$ point, there is a Shockley state about 184 mRy above zero within the Δ_1 hybridization gap.[73] A Tamm state has been observed at 425 mRy nearly above the flat Z_2 band, which has already been mentioned above.[70] Furthermore, at $\bar{X}$ two occupied surface states are known at about 226 mRy (Ref. 73) and 557 mRy (4 mRy below E_F);[105] there is also a resonance at $\bar{X}$ situated just on the band edge (L_1) above E_F.[75] An unoccupied $\bar{\Gamma}$ surface state has been reported at about 850 mRy.[106,107,75] It was quite surprising for the author that, despite the simplified theoretical model, this spectrum of experimental data was not only qualitatively reproduced by his calculations, but also quantitatively (with the exception of the unoccupied $\bar{\Gamma}_1$ state). A vacuum potential barrier with $z_w=0$ and $L\approx 0.2$ a.u. yields differences of 2–12 mRy between calculated and measured surface-state energies (see Fig. 6); only the $\bar{\Gamma}_1$ state, which is located at a complex loop extending from the X_4' to the X_1 bulk state over a height of 400 mRy, differs from the experimental value by at least 90 mRy, although it is very sensitive to a variation of z_w and L.[108]

Thus, it may be concluded that—in contrast to other assertions[109]—an adequate description of crystal-induced surface states does not primarily require self-consistency in the calculation of the electronic potential.[110] It seems much more important to use a bulk potential which is able to reproduce the electronic properties of the infinite crystal as accurately as possible; furthermore, it must be emphasized that the use of reliable mathematical methods is crucial when designing a physically reasonable model. Only if those surface properties which are essentially determined by the crystal substructure can be numerically mastered without difficulties (especially with regard to convergence and accuracy), should the self-consistent calculation of effects be attacked which influence the details of the electronic potential in the vacuum and the surface region. One cannot but guess that negligence of these conclusions may be the cause for the rather considerable discrepancies between the results of some other calculations of surface states (Refs. 111, 18, 9, 112, 113, 57, and 4) based on different models and alternative methods, and also for the differences they exhibit when compared to the experimental data.

ACKNOWLEDGMENTS

I would like to thank Professor H. Bross for encouraging me to do this work and supporting it by many useful discussions. I am also grateful to Dr. H. Stoehr for providing me with the subroutines solving Schrödinger's equation in the vacuum region. The numerical calculations were performed at the Leibniz Rechenzentrum der Bayerischen Akademie der Wissenschaften in Munich. This work was supported by Deutsche Forschungsgemeinschaft, under Sonderforschungsbereich 128.

[1] D. W. Bullett, J. Phys. C **11**, 4501 (1978); **14**, 4521 (1981).

[2] E. E. Lafon, R. C. Chaney, and C. L. Chun, in *Computational Methods in Band Theory*, edited by P. M. Marcus, J. F. Janak, and A. R. Williams (Plenum, New York, 1971), pp. 284–295.

[3] J. A. Appelbaum and D. R. Hamann, Solid State Commun. **27**, 881 (1978).

[4] A. Euceda, D. M. Bylander, L. Kleinman, and M. Kenneth, Phys. Rev. B **27**, 659 (1983).

[5] O. K. Andersen and R. V. Kasowski, Phys. Rev. B **4**, 1064 (1971).

[6] O. K. Andersen, Phys. Rev. B **12**, 3060 (1975).

[7] R. V. Kasowski, Solid State Commun. **17**, 179 (1975).

[8] O. Jepsen, J. Madsen, and O. K. Andersen, Phys. Rev. B **18**, 605 (1978).

[9] H. Krakauer, M. Posternak, and A. J. Freeman, Phys. Rev. B **19**, 1706 (1979).

[10] P. M. Marcus and D. W. Jepsen, Phys. Rev. Lett. **20**, 925 (1968).

[11] D. W. Jepsen and P. M. Marcus, in *Computational Methods in Band Theory*, edited by P. M. Marcus, J. F. Janak, and A. R. Williams (Plenum, New York, 1971), pp. 416–443.

[12] J. A. Appelbaum and D. R. Hamann, Phys. Rev. B **6**, 2166

(1972).
[13]E. G. McRae, Surf. Sci. 11, 479 (1968).
[14]D. W. Jepsen, Phys. Rev. B 22, 5701 (1980).
[15]G. Wachutka, Ph.D. thesis, Ludwig-Maximilians-Universität, München, 1985 (unpublished).
[16]G. Wachutka, Ver. Dtsch. Phys. Ges. (VI) 19, 340 (1984).
[17]H. Bross, J. Phys. F 12, 2883 (1982).
[18]D. Spanjaard, D. W. Jepsen, and P. M. Marcus, Phys. Rev. B 19, 642 (1979).
[19]N. A. W. Holzwarth and M. J. G. Lee, Phys. Rev. B 18, 5350 (1978).
[20]G. Wachutka, Diplomarbeit, Ludwig-Maximilians-Universität, München, 1978 (unpublished).
[21]K. Kambe, Z. Naturforsch. Teil A 22, 322 (1967); 22, 422 (1967); 23, 1280 (1968).
[22]J. B. Pendry, *Low Energy Electron Diffraction* (Academic, London, 1974).
[23]M. A. Van Hove and S. Y. Tong, *Surface Crystallography by LEED* (Springer, Berlin, 1979).
[24]R. Hora and M. Scheffler, Phys. Rev. B 29, 692 (1984).
[25]J. B. Pendry, Surf. Sci 57, 679 (1976).
[26]See Eqs. (31)–(33) in the second paper cited in Ref. 21.
[27]E. Tamura and R. Feder, Ver. Dtsch. Phys. Ges. (VI) 18, 801 (1983).
[28]Apart from a discrete set of energy values, which are the eigenvalues of the monolayer problem.
[29]See Sec. IV. F of Ref. 22.
[30]See Chap. 8 in Ref. 23.
[31]V. Heine, Proc. Phys. Soc. 81, 300 (1963).
[32]Among various approaches to generalized Bloch waves [see, e.g., Refs. 13, 11, 22, 19, 17, and also Y. C. Chang and J. N. Schulman, Phys. Rev. B 25, 3975 (1982); 27, 2346 (1983)] the eigenvalue problem (5) seems to provide the most direct way to calculate the real lines of the complex band structure. In contrast to other methods which also make use of a linear eigenvalue problem for $\exp(i\mathbf{k}\cdot\mathbf{a}_3)$, the formulation given here ensures stable results with well-defined accuracy, since it is not based on the propagation matrix. Besides, it enables the calculation of the bulk band structure in the case of more complicated layered structures which lie beyond the capabilities of the usually applied methods [e.g., L.F. Mattheiss, Phys. Rev. B 8, 3719 (1973); J. Robertson, J. Phys. C 12, 4753 (1979); S. P. Hind and P. M. Lee, *ibid.* 13, 349 (1980); A. Šimůnek and G. Wiech, Phys. Rev. B 30, 923 (1984)].
[33]H. Bross, Z. Phys. B 28, 173 (1977).
[34]M. von Laue, Phys. Rev. 37, 53 (1931).
[35]M. Reed and B. Simon, *Methods of Modern Mathematical Physics* (Academic, New York, 1972), Vol. I, theorem VI. 17.
[36]J. H. Wilkinson, in *Numerical Software—Needs and Availability*, edited by D. A. H. Jacobs (Academic, New York, 1978).
[37]J. A. Appelbaum and D. R. Hamann, Rev. Mod. Phys. 48, 479 (1976).
[38]D. W. Jepsen, Phys. Rev. B 20, 402 (1979).
[39]J. C. Slater, Phys. Rev. 51, 151 (1937).
[40]T. Loucks, *Augmented Plane Wave Method* (Benjamin, New York, 1967).
[41]See, G. Wachutka and H. Bross, J. Phys. A 15, 3083 (1982); a variational expression adapted to the monolayer problem is obtained by setting $u := w := -\Lambda$; $f_0^{(0)} := g_0^{(0)} := 0$; $f_0^{(1)} := g_0^{(1)} := b$ in Eq. (A4.5).
[42]*Handbook of Mathematical Functions,* edited by M. Abramowitz and I. A. Stegun (Dover, New York, 1965).
[43]Y. L. Luke, *The Special Functions and Their Approximations* (Academic, New York, 1969), Vol. I, Sec. 8.5.3.
[44]I. S. Gradshteyn and I. M. Ryzhik, *Table of Integrals, Series and Products* (Academic, New York, 1965).
[45]J. F. Hart, *Computer Approximations* (Wiley, New York, 1968).
[46]W. Gautschi, Commun. ACM 7, 479 (1964).
[47]See Y. L. Luke, *The Special Functions and Their Approximations,* Ref. 43, Vol. I, p. 309.
[48]D. J. Chadi and M. L. Cohen, Phys. Rev. B 8, 5747 (1973).
[49]S. L. Cunningham. Phys. Rev. B 10, 4988 (1974).
[50]H. J. Monkhorst and J. D. Pack, Phys. Rev. B 13, 5188 (1976).
[51]A. H. MacDonald, Phys. Rev. B 18, 5897 (1978).
[52]H. Bross, J. Phys. F 8, 2631 (1978).
[53]C. B. Moler and G. W. Stewart, SIAM J. Numer. Anal. 10, 241 (1973).
[54]R. C. Ward, U.S. National Aeronautics and Space Administration Technical Note No. NASA-TN-D-7305, 1973 (unpublished).
[55]L. C. Kaufmann, ACM Trans, Math, Software 1, 271 (1975).
[56]J. H. Wilkinson, National Physical Laboratory (Teddington, England) Report No. DNACS-10/78, 1978 (unpublished).
[57]J. R. Smith, J. G. Gay, and F. J. Arlinghaus, Phys. Rev. B 21, 2201 (1980).
[58]A discontinuity of $\kappa_{\min}(E)$ is to be expected if the number $2\sigma(E)$ of propagating waves changes its value.
[59]E. C. Snow, Phys. Rev. 158, 683 (1967).
[60]M. I. Chodorow, Ph.D. thesis, Massachusetts Institute of Technology, 1939 (unpublished).
[61]G. A. Burdick, Phys. Rev. 129, 138 (1963).
[62]D. W. Jepsen, P. M. Marcus, and F. Jona, Phys. Rev. B 5, 3933 (1972).
[63]K. Kambe, in *Computational Methods in Band Theory,* edited by P. M. Marcus, J. F. Janak, and A. R. Williams (Plenum, New York, 1971), pp. 409–415.
[64]J. S. Faulkner, Phys. Rev. 178, 914 (1969).
[65]P. O. Gartland and B. J. Slagsvold, Solid State Commun. 25, 489 (1978).
[66]S. J. Gurmann and J. B. Pendry, Phys. Rev. Lett. 31, 637 (1973).
[67]P. O. Gartland and B. J. Slagsvold, Phys. Rev. B 12, 4047 (1975).
[68]S. J. Gurmann, J. Phys. C 9. L609 (1976).
[69]J. Stoehr *et al.*, Phys. Rev. B 17, 587 (1978).
[70]P. Heimann, J. Hermanson, H. Miosga, and H. Neddermeyer, Phys. Rev. B 20, 3059 (1979).
[71]E. Louis and J. A. Vérges, J. Phys. F 10, 207 (1980).
[72]P. Durham and N. Kar, Surf. Sci. 111, L648 (1981).
[73]D. Westphal and A. Goldmann, Surf. Sci. 131, 92 (1983).
[74]W. Altmann *et al.*, Phys. Rev. B 29, 3015 (1984).
[75]V. Dose, U. Kolac, G. Borstel, and G. Thoerner, Phys. Rev. B 29, 7030 (1984).
[76]J. A. Knapp, F. J. Himpsel, and D. E. Eastman, Phys. Rev. B 19, 4952 (1979).
[77]P. Thiry *et al.*, Phys. Rev. Lett. 43, 82 (1979).
[78]Y. Pétroff and P. Thiry, Appl. Opt. 19, 3957 (1980).
[79]G. Thoerner and G. Borstel, Solid State Commun. 47, 329 (1983).
[80]J. F. Janak, A. R. Williams, and V. L. Moruzzi, Phys. Rev. B 11, 1522 (1975).
[81]V. L. Moruzzi, A. R. Williams, and J. F. Janak, *Calculated Electronic Properties of Metals* (Pergamon, New York, 1978).
[82]H. B. Michaelson, J. Appl. Phys. 48, 4729 (1977).
[83]N. D. Lang and W. Kohn, Phys. Rev. B 1, 4555 (1970).
[84]H. Stoehr and H. Bross, Surf. Sci. 124, 99 (1983).
[85]F. Szmulowicz and B. Segall, Phys. Rev. B 24, 892 (1981).

[86]Note the corrections made by F. C. Greisen, Phys. Status Solidi **25**, 753 (1968).
[87]S. Y. Tong and M. A. Van Hove, Phys. Rev. B **16**, 1459 (1977).
[88]J. B. Pendry and F. Forstmann, J. Phys. C **3**, 59 (1970).
[89]P. M. Marcus and D. W. Jepsen, *Computational Methods for Large Molecules and Localized States in Solids,* edited by F. Herman, A. D. McLean, and R. K. Nesbet (Plenum, New York, 1972), p. 235.
[90]C. Herring, Phys. Rev. **52**, 365 (1937).
[91]W. Kohn, Phys. Rev. **115**, 809 (1959).
[92]See M. Reed and B. Simon, *Methods of Modern Mathematical Physics,* Ref. 35, Vol. IV, Chap. XIII.16.
[93]J. E. Avron and B. Simon, Ann. Phys. **110**, 85 (1978).
[94]I. Tamm, Z. Phys. **76**, 849 (1932).
[95]A. W. Maue, Z. Phys. **94**, 717 (1935).
[96]W. Shockley, Phys. Rev. **56**, 317 (1939).
[97]F. Forstmann, Z. Phys. **235**, 69 (1970).
[98]F. Forstmann and J. B. Pendry, Z. Phys. **235**, 75 (1970).
[99]F. Forstmann and V. Heine, Phys. Rev. Lett. **24**, 1419 (1970).
[100]P. M. Echenique and J. B. Pendry, J. Phys. C **11**, 2065 (1978).
[101]J. B. Pendry and S. J. Gurman, Surf. Sci. **49**, 87 (1975).
[102]G. V. Hansson and S. A. Flodström, Phys. Rev. B **18**, 1562 (1978).
[103]H. J. Levinson, F. Greuter, and E. W. Plummer, Phys. Rev. B **27**, 727 (1983).
[104]M. Seel, Phys. Rev. B **28**, 778 (1983).
[105]S. D. Kevan, Phys. Rev. B **28**, 2268 (1983).
[106]P. D. Johnson and N. V. Smith, Phys. Rev. B **27**, 2527 (1983).
[107]D. Straub and F. J. Himpsel, Phys. Rev. Lett. **52**, 1922 (1984).
[108]This agrees with the observations made in Ref. 75.
[109]F. J. Arlinghaus, J. G. Gay, and J. R. Smith, in *Theory of Chemisorption,* Vol. 19 of *Topics in Current Physics,* edited by J. R. Smith (Springer-Verlag, Berlin, 1980), pp. 71—114.
[110]A similar thesis has been stated by Bullett (see the second paper cited in Ref. 1).
[111]E. Caruthers, L. Kleinman, and G. P. Alldredge, Phys. Rev. B **8**, 4570 (1973).
[112]R. V. Kasowski, Phys. Rev. Lett. **33**, 83 (1974).
[113]D. G. Dempsey and L. Kleinman, Phys. Rev. B **16**, 5356 (1977).